

An LUT-Based Inversion of DART Model to Estimate Forest LAI from Hyperspectral Data

Asim Banskota, Shawn P. Serbin, Randolph H. Wynne, Valerie A. Thomas, Michael J. Falkowski, Nilam Kayastha, Jean-Philippe Gastellu-Etchegorry, and Philip A. Townsend

Abstract—The efficient inversion of complex, three-dimensional (3-D) radiative transfer models (RTMs), such as the discrete anisotropy radiative transfer (DART) model, can be achieved using a look-up table (LUT) approach. A pressing research priority in LUT-based inversion for a 3-D model is to determine the optimal LUT grid size and density. We present a simple and computationally efficient approach for populating an LUT database with DART simulations over a large number of spectral bands. In the first step, we built a preliminary LUT using model parameters with coarse increments to simulate reflectance for six broad bands of Landsat Thematic Mapper (TM). In the second step, the preliminary LUT was compared with the TM reflectance, and the optimal input ranges and realistic parameter combinations that led to simulations close to Landsat spectra were then identified. In the third step, this information was combined with a sensitivity study, and final LUTs were built for the full spectrum of Airborne Visible/Infrared Imaging Spectrometer (AVIRIS) narrow bands and six Landsat broad bands. The final LUT was inverted to estimate leaf area index (LAI) in northern temperate forests from AVIRIS and TM data. The results indicate that the approach used in this study can be a useful strategy to estimate LAI accurately by DART model inversion.

Index Terms—Hyperspectral remote sensing, imaging spectrometer, inversion methods, Landsat, look-up-table (LUT), radiative transfer.

I. INTRODUCTION

THE leaf area index (LAI, m^2m^{-2}) of vegetation canopies controls and moderates different climatic and ecological functions [1]–[6]. Since LAI is one of the principal factors influencing canopy reflectance [7], a large body of research has investigated the use of airborne and satellite remote sensing data for its accurate retrieval over broad landscapes [8]–[16]. A common approach for estimating LAI is to employ empirically-based statistical techniques, which are generally site-specific or difficult to parameterize over broad regions [17]–[19]. In contrast, a mechanistic, physically-based approach using canopy radiative transfer model (RTM) is based on our best understanding of the physical laws governing the transfer and the interaction of solar radiation in a vegetative canopy. With sufficient complexity, RTMs can be extended over areas with different environmental conditions and canopy structure characteristics (e.g., broadleaf, needle-leaf, and grassland), and is better suited for many large-scale applications [17], [19]–[24]. Physically-based methods can also make full use of the high dimensional spectral and multiangular information provided by many modern sensors [24], [25].

Physically-based RTMs range from a simple one-dimensional (1-D) to a more complex three-dimensional (3-D) models. 1-D models assume that canopies vary only with the height above the ground surface but are homogenous in the horizontal direction [3]. However, most plant stands contain the partial cover and generally exhibit horizontal variability in their structural and optical properties, and are thus may be imprecisely modeled using 1-D models depending on the spatial scale of interest. A more realistic description of forest canopy-reflected radiation can be provided by 3-D models [6], [20], [26]–[29], however, at the expenses of computational complexity and increased parameterization challenges [3]. The models are referred to as 3-D because the extinction and scattering coefficients that define photon interactions are explicit functions of the spatial coordinates [29]. Additionally, there are families of geometric-optical models such as Li-Strahler [30] and five-scale models [31] that specify coefficients in three dimensions based on some parametrized statistical distribution models rather than specifying the photon interactions explicitly.

Manuscript received September 15, 2014; revised December 18, 2014; accepted January 26, 2015. The work of A. Banskota was supported in part by the Graduate School at Virginia Tech (Geospatial and Environmental Analysis Program, College of Natural Resources and Environment), in part by the NASA New Investigator Program under Grant NNX14AC26G, and in part by the NASA Terrestrial Ecology Program under Grant NNX14AF96G. The work of S. Serbin and P. Townsend was supported in part by NASA Earth and Space Science Fellowship under Grant NX08AV07H and in part by NASA Terrestrial Ecology under Grant MNX08AN31G.

A. Banskota and N. Kayastha were with Geospatial and Environmental Analysis Program, Virginia Polytechnic Institute and State University, Blacksburg, VA 24061 USA. They are now with the Department of Forest Resources, University of Minnesota, Minneapolis, MN 55108 USA.

S. P. Serbin was with the Department of Forest and Wildlife Ecology, University of Wisconsin-Madison, Madison, WI 53706 USA. He is now with the Department of Biological, Environmental, and Climate Sciences, Brookhaven National Laboratory, Upton, NY 11973 USA.

R. H. Wynne and V. A. Thomas are with the Department of Forest Resources and Environmental Conservation, Virginia Polytechnic Institute and State University, Blacksburg, VA 24061 USA.

M. J. Falkowski is with the Department of Forest Resources, University of Minnesota, Minneapolis, MN 55108 USA (e-mail: banskota@umn.edu).

J.-P. Gastellu-Etchegorry is with the Centre d'Etudes Spatiales de la Biosphère—CNES, CNRS, IRD, Université de Toulouse III—Paul Sabatier, Toulouse 31062, France.

P. A. Townsend is with the Department of Forest and Wildlife Ecology, University of Wisconsin-Madison, Madison, WI 53706 USA.

Color versions of one or more of the figures in this paper are available online at <http://ieeexplore.ieee.org>.

Digital Object Identifier 10.1109/JSTARS.2015.2401515

The discrete anisotropy radiative transfer (DART) model is a widely used 3-D model in remote sensing research [6], [32]–[34]. DART uses simplifying hypotheses for simulating vegetation landscapes by dividing the scene into rectangular cells characterized by the volume and scattering properties of landscape elements. As with other 3-D RTMs, DART contains a large suite of input parameters; however, some of these have a lower impact on modeled reflectance than others. Parameters that have a small influence [based on existing knowledge or sensitivity analysis (SA)] can be represented as constants, ultimately lowering the dimensionality of the model inversion [26]. Since its release [26], the accuracy, range of applications, and graphical user interface of DART have been significantly improved [6], [32]. It was compared and tested within the European Commission Radiation Transfer Model Intercomparison (RAMI) experiment [35]. The experiment indicated that DART simulations of heterogeneous canopy spectra were in close agreement with the simulations from other 3-D candidate models such as FLIGHT, Rayspread, Raytran, and Sprint3 [34]. A detailed description of the DART model is provided in [26] and [27].

RTM inversion for important biophysical parameter, such as LAI, requires the efficient comparison of observed against modeled spectral optical properties across a range of wavelengths, pixel sizes, vegetation types, and spatial domains. Several model inversion techniques are available [36]–[38]. Traditional methods such as optimization techniques iteratively adjust model parameters until the modeled reflectance “fits” or match the measured signal. Such approaches require significant computing resources for a large number of spectral channels or spatial domain and are generally much less computationally efficient to operate on a per-pixel basis [37].

Computationally efficient statistical inversion approaches such as neural network can be used to train models to invert the signal [36]–[38]. The major drawbacks of neural network include time-consuming training phase and the unpredictable behavior when the characteristics of the targets are not well represented by the modeled spectra [38]. Look-up table (LUT)-based inversion methods in which a database of “solutions” is precalculated as a function of input parameters are also widely used in remote sensing applications [25], [39]–[42]. In this approach, the observed image spectrum is compared with simulated spectra in the LUT database, and the closest match, or an ensemble of close matches, is found. The parameter combination that yields the closest spectra in the database [32], or a summary statistic of ensemble matches [43], is considered the inversion solution [44]. The major advantage of the LUT-based approach over the iterative optimization approaches is that the forward modeling is divorced from the inversion procedure, and hence can be used for any complex model like DART [27], [46]. If a suitable LUT is built, it can be used to invert spectra across a range of conditions. A key problem is to identify a suitable range and appropriate number of cases (incremental steps) for parameters to keep the size of the LUT as small as possible. The incremental steps should be fine enough to achieve a high degree of precision for the estimated parameters [43]–[46]. This requires a large number

of model simulations for a single reflectance band, which is significantly cost prohibitive in the case of a 3-D model like DART and practically infeasible for hyperspectral bands; however, this computational cost is divorced from the inversion step and is done once.

Peddle *et al.* [48] suggested a two-stage process to initially produce a table based on wide ranges and coarse increments to identify the general range of the model inputs producing reflectance values similar to those of the remote sensing image. The output can then be used to identify narrower input ranges where matches occurred, for which a final table can be produced with fine increments. Such a two-stage process might help find the optimal input range for DART parameters, but does not inform users about the appropriate incremental steps. Furthermore, not all parameter combinations within the identified range produce output similar to the image reflectance. Identification of such infeasible combinations might significantly reduce the computation time for DART. Banskota *et al.* [49] developed an efficient strategy for building an LUT for Airborne Visible/Infrared Imaging Spectrometer (AVIRIS) hyperspectral bands using plot-extracted spectra to constrain the LUT size and grid density. The plot spectra were sampled across a range of temperate deciduous forests in the Northern United States. Such requirement of plot spectra limits the geographical scope of the LUT and also makes the approach empirical in nature. In this follow-on study, we build on the approach by substituting the Landsat image spectra for plot spectra to expand the scope of the method in regional and broader applications. We tested our new strategy for building an LUT of DART-simulated reflectances for AVIRIS and Landsat bands, and compared the utility of the sensors for estimating LAI via the LUT approach.

II. METHODS

A. Study Area

This study area is the same as Banskota *et al.* [49] and comprises a broad range of broadleaf deciduous forest types within the state of Wisconsin, USA. Briefly, the northern-most forest sites were located within the Northern Lakes and Forest ecoregion, dominated by a mixed-hardwood forest originating from the large-scale clear-cut practices of the early 20th century [51]. The southern sites were located in the Baraboo Hills of the “Driftless” (unglaciated) ecoregion of Wisconsin.

B. LAI Measurement Protocol

We used the same field dataset as Banskota *et al.* [49], which describes the detailed measurement and processing protocol. Briefly, hemispherical images were collected at 18 plots (60 m × 60 m) characterized by broadleaf deciduous forest types. Optical measurements of effective LAI (L_e) were estimated from these photos collected at 1 m above the forest floor using a Nikon CoolPix 5000 digital camera, leveled on a tripod with an attached Nikon FC-E8 183° lens [52]–[54]. Understory (i.e., vegetation below 1 m height) was not included

in our measurements as this was generally pretty minimal at our plot locations. L_e represents the equivalent leaf area of a canopy with a random foliage distribution to produce the same light interception as the true LAI [55], [56] and is derived from the canopy gap fraction at selected zenith angles beneath the canopy following Leblanc *et al.* [5]

$$\text{LAI} = \frac{L_e}{\Omega} (1 - \alpha) \quad (1)$$

where L_e is the effective LAI, Ω is the clumping index, and α is the woody-to-total leaf area ratio ($\alpha = W/L_e (1/\Omega)$), in which W represents the woody-surface-area-index (half the woody area m^{-2} ground area). In this study, we calculated LAI from L_e by correcting the effect of clumping but neglecting the effect of woods and branches in (1) (i.e., $\text{LAI} = L_e/\Omega$).

Banskota *et al.* [49] identified one plot data with the highest LAI value (6.67) as outlier and did not include the plot in final analysis. Unlike the precursor study, we did not use plot data to constrain LUT simulation. Hence, our method is not sensitive to errors in plot measurement, and therefore we included all the 18 plots in this study.

C. Image Collection and Processing

The AVIRIS data used in this study were acquired in July, 2008 on NASA's ER-2 aircraft at an altitude of 20 km, yielding a pixel (i.e., spatial) resolution of approximately 17 m (16.8–17.0 m). The AVIRIS instrument produces 224 spectral bands (or wavelengths), with an approximate full-width half-maximum of 10 nm for each wavelength over the spectral range from 370 to 2500 nm [57]. AVIRIS image preprocessing involved manual delineation of clouds and cloud-shadows, cross-track illumination correction, and conversion to top-of-canopy (TOC) reflectance via atmospheric correction [50]. Atmospheric correction of the cross-track illumination-corrected images to TOC reflectance employed the ACORN5bTM software (Atmospheric CORrection Now; Imspec LLC, USA). ACORN provides the choice for user-selectable parameters for visibility and standard aerosol model. We selected rural temperate aerosol model and used fixed visibility information obtained from the closest meteorological station. ACORN used two water absorption channels (940 and 1140 nm) in AVIRIS data to estimate the amount of water vapor at the time of acquisition.

Due to the low ratio of signal to noise (SNR) at both spectral ends (366–395 and 2467–2497 nm), and in bands around the major water absorption regions (1363–1403 and 1811–1968 nm), those wavelength regions were removed, resulting in a final total of 184 bands for our analysis.

Two Landsat TM surface reflectance products (Path/Row = 25/28: Julian date 2009250 and Path/row = 26/28: Julian date 2009273) from the Landsat surface reflectance climate data record were downloaded from the United States Geological Survey (USGS) EarthExplorer site (<http://earthexplorer.usgs.gov/>). Images from 2009 were used as cloud-free 2008 summer imagery over ground plots were not available, and we did not see any major disturbances or changes as compared to the AVIRIS images. Landsat

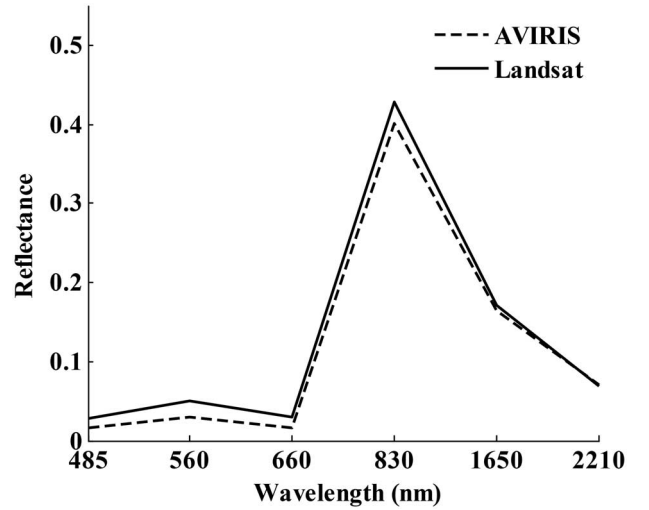


Fig. 1. Landsat versus AVIRIS (six narrow bands) pixel spectra extracted over one of the study plots (LAI = 5.4).

surface reflectance climate data records are generated from the Landsat Ecosystem Disturbance Adaptive Processing System (LEDAPS) software, which employs the 6S RTM [58]. The program estimates per-pixel AOT using the dense dark vegetation (DDV) method and retrieves other ancillary data from various sources that include the Total Ozone Mapping Spectrometer (TOMS) data, column water vapor from the NOAA National Centers for Environmental Prediction (NCEP) reanalysis data, digital topography, and NCEP surface pressure data. The images we employed were processed to Level 1 terrain corrected (L1T) format, which have undergone systematic radiometric and geometric corrections [59].

Both Landsat scenes and AVIRIS images were independently georegistered with subpixel accuracy. We visually examined the coordinate mismatch between Landsat scenes and AVIRIS images and no discrepancy among two dataset was observed. The pixel spectra corresponding to the centers of the plot locations were extracted from AVIRIS and Landsat images. Fig. 1 shows the extracted spectra for Landsat TM bands and corresponding six narrow bands from one of the study plots (LAI = 5.4), which shows that the visible reflectance was higher in the Landsat than AVIRIS spectra. Such discrepancies in the visible reflectance were consistent for all the 18 plots. The different atmospheric procedures applied for two images might be attributable to such discrepancies. ACORN, employed a default aerosol model (temperate rural) and may have overcorrected the atmospheric effects in the AVIRIS bands compared to 6S model that used DDV approach to estimate aerosol optical thickness in the Landsat image. However, ACORN is a commonly used approach and the differences may just be related to the different assumptions between ACORN and 6S.

D. DART Scene Formulation

We used DART version 4.3.3 to simulate the LUT canopy bidirectional reflectance factor (BRF: from herein referred to as reflectance). The DART model was run in a UNIX environment using a computer with 32 central processing units (eight

Quad-Core AMD Opteron™ 8356 Processor) and 64 GB of physical random access memory (RAM). However, conversely to the new DART 5.5.1 version, DART version 4.3.3 was not multithreaded, which constrained us to use one processing at a time. In order to simulate the reflectance of any landscape such as a forest or an urban area, DART requires users to build a computer representation of that landscape. Ideally, the scene area should be large and should include important details about the landscape. For instance, a forest scene should be built with a large number of trees, and the resolution of the scene (cell) should be high enough to represent canopy elements such as leaves, twigs, and branches. This level of detail leads to an unacceptable computational time when building an LUT for image inversion. Thus, a scene of reasonable size and detail needs to be determined that allows one to operate the DART model with an acceptable accuracy level. In this study, simulations were conducted using a repetitive forest landscape pattern made up of four trees with ellipsoid-shaped crowns; previous studies have found this representation to be optimal [27], [30]. The trees were described by constant below crown (6 m) and within-crown height (9 m). Both the scene size (20–30 m) and the dimension of the tree crowns (major and minor axes: 5–10 m) were varied to obtain scenes of different ground cover. The scenes were built using unitary cells of 1 m × 1 m × 1 m resolution. The canopy was represented by foliage with trunks, and without woody branches and twigs. The architecture of woody elements was not well known; therefore, we did not include this level of detail to avoid introducing additional uncertainties. As shown in Appendix I, we found that such simulation in the absence of branches and twigs has negligible effect on the reflectance especially at high LAI (relative error less than 1% of the reflectance when the ground LAI is equal to or greater than 4).

E. LUT Generation

Two LUT databases populated with AVIRIS and Landsat reflectance information were created in three separate steps. First, a preliminary LUT was built with DART simulations for six Landsat TM bands using a wide range and coarse increments for parameters. In the second step, simulations in the preliminary LUT were compared to the maximum and minimum band reflectances of broadleaf vegetation in Landsat images, and those simulations within the range of image spectra were retained. By analyzing parameter values in the reduced LUT, a list of useful parameter combinations that produce reflectance values within the range of image spectra were identified. Based on the results of an SA, optimal input increments were determined. Finally, LUTs were built for 6 Landsat bands and 184 narrow AVIRIS bands using the identified list of useful parameter combinations and incremental levels. A conceptual diagram for the LUT building process is shown in Fig. 2, and the three steps are discussed below in detail. PROSPECT-4 [60], integrated with DART 4.3.3, was used to calculate leaf optical properties (reflectance and transmittance). The PROSPECT-4 calculates leaf hemispherical transmittance and reflectance over the solar spectrum from 400 to 2500 nm

as a function of four input parameters: 1) leaf structural parameter (N); 2) leaf chlorophyll a + b concentration (Cab); 3) leaf dry matter content (DM); and 4) equivalent water thickness (EWT).

1) *Computation of Preliminary LUT*: DART reflectance was simulated for the bandwidth defined by six Landsat TM bands (450–520, 530–600, 630–690, 760–900, 1550–1750, and 2080–2350 nm). The parameters that were varied were four PROSPECT parameters (Cab, DM, N, and EWT), LAI, leaf angle distribution (LAD), soil reflectance (SL), and canopy cover (CC). A fixed value for fraction of diffuse incoming solar radiation (0.1) was used across all wavelengths, as previously done in other studies [38]. The simulations were conducted for a single solar angle associated with an AVIRIS scene as we found little variation among canopy reflectance at different solar angles associated with the AVIRIS and Landsat scenes in this study. The parameters, their ranges, and the incremental steps are listed in Table I, which were kept reasonably wide and coarse to minimize simulation time in the preliminary step. The four LADs used were erectophile, planophile, plagiochile, and extremophile distributions [61].

2) *Search for Realistic Parameter Combinations and SA*: We compared the preliminary LUT simulations with the spectra of broadleaf deciduous vegetation from two Landsat scenes to determine optimal parameter combinations and ranges. Deciduous cover types in the Landsat scenes were identified using the most recent national land cover product from the Multi-Resolution Land Characteristics (MRLC) Consortium (<http://www.mrlc.gov/nlcd2011.php>). We determined the maximum and minimum reflectance band values corresponding to deciduous pixels in both sets of images and combined to form a maximum and a minimum reflectance (max/min) spectrum. A search filter was then applied to find the LUT simulations confined within the max/min space. Model inputs that led to simulations (candidate solutions) in the reduced LUT were examined to infer information about optimal ranges and realistic parameter combinations. The iterative procedure to identify such optimal parameter combinations is further described in Appendix II.

A simple univariate SA was performed as in [62] and [63] to determine the importance of each parameter and the optimal discretization of parameters within their identified ranges. Each parameter was perturbed in turn keeping all other model parameters fixed at their reference values (base case). Equal numbers of perturbation values with equal relative intervals were used for all parameters (Table II). The process was performed for the same set of bands previously used to compute the preliminary LUT. A merit function F' was computed using (2) and called sensitivity

$$F' = \sum_{\text{pert}=1}^n \frac{(\rho_{0j} - \rho_{\text{pert}j})^2}{\rho_{0j}} \quad (2)$$

where ρ_o is the base reflectance, ρ_{pert} is the perturbed reflectance in band j , and n is the total number of perturbations.

Based on the SA results, the optimal number of cases for each parameter was determined such that the number of

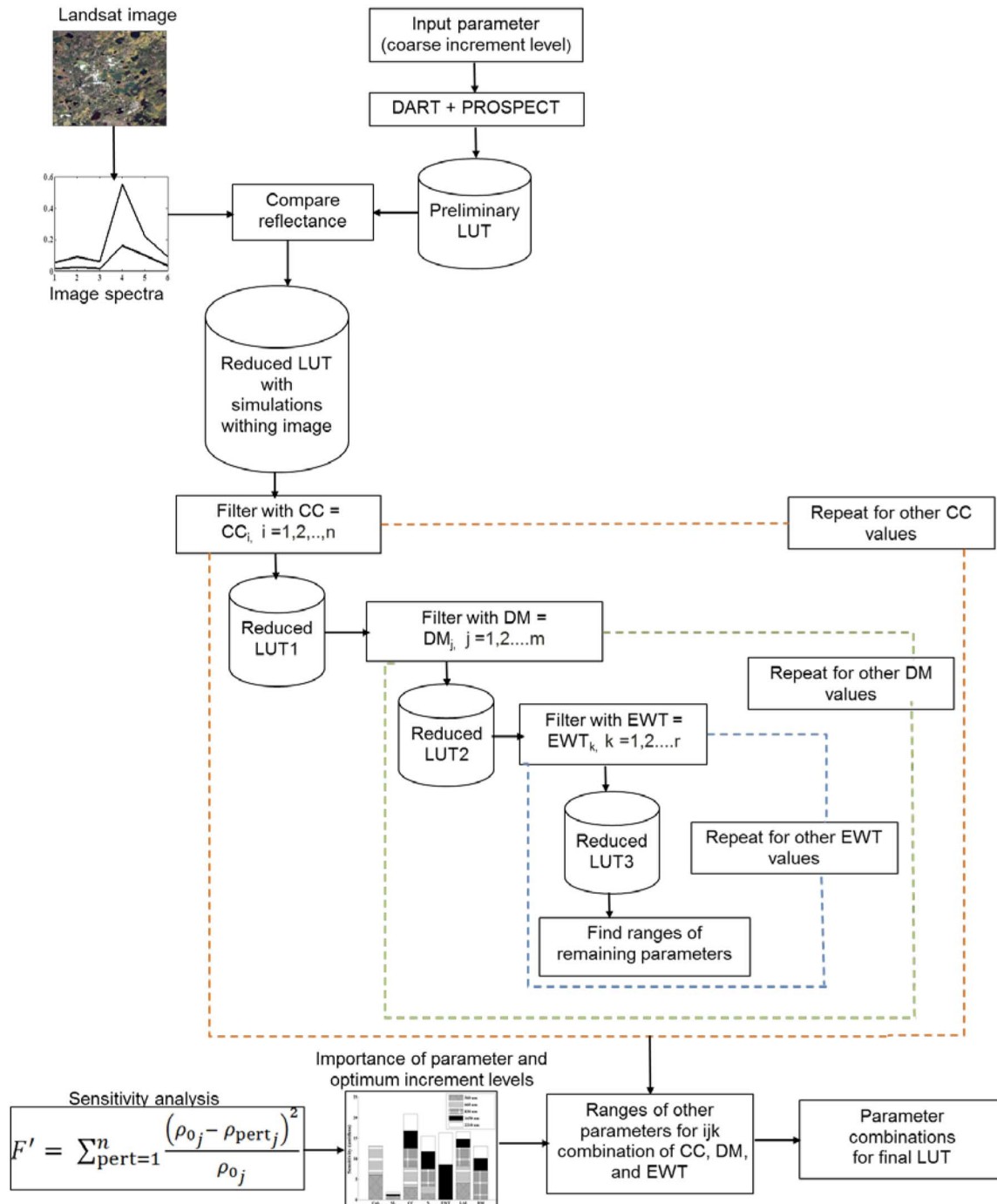


Fig. 2. Conceptual framework for the LUT building technique used. CC refers to canopy cover (%), DM refers to leaf dry matter content (g/cm^{-2}), EWT refers to leaf equivalent water thickness (cm). Sensitivity F' was calculated using a base reflectance (ρ_0) and the perturbed reflectance (ρ_{pert}) in band j , and n number of perturbations.

cases was proportional to the corresponding greatest magnitude of the sensitivity. The effects of four different LADs on canopy reflectance were visually assessed by plotting the reflectance with four LADs at constant values of other parameters.

Independent LUTs for 6 Landsat broad bands and 184 narrow AVIRIS bands were built on the basis of optimal parameter combinations and input increments determined in the previous stages.

3) *LUT Inversion*: LUT inversion involved matching the similarity between plot spectra (measured) and simulated spectra (modeled). Spectrum matching was performed using a least root mean square error (RMSE) comparison of the measured and modeled spectra according to (3)

$$\text{RMSE} = \sqrt{\frac{\sum_{i=1}^n (R_{\text{measured}} - R_{\text{modeled}})^2}{n}} \quad (3)$$

TABLE I
DART + PROSPECT PARAMETERS, THEIR RANGES, AND INCREMENTS
USED IN PRELIMINARY LUT BUILDING

Parameters	Minimum	Maximum	Increment
LAI (m ² /m ²)	1	7	1
EWT (cm)	0.001	0.018	0.003
DM (g/cm ²)	0.001	0.041	0.005
N	1.5	4	0.5
Cab (μg/cm ²)	10	70	10
CC (%)	50	100	25
SL (%)	10	40	15

The parameters are LAI, leaf EWT, leaf DM, leaf structural parameter (N), leaf CAB concentration, CC, and SL.

TABLE II
BASE CASES AND THE RANGE OF PERTURBATIONS FOR THE
PARAMETERS CONSIDERED IN THE SENSITIVITY ANALYSIS

Parameters	Base-case	Range of perturbations
LAI (m ² /m ²)	4	1-7
EWT (cm)	0.01	0.001–0.018
DM (g/cm ²)	0.01	0.001–0.04
N	2.5	1.5–4
Cab (μg/cm ²)	40	10–70
CC (%)	80	50–100
SL (%)	20	10–40

The parameters are LAI, leaf EWT, leaf DM, leaf structural parameter (N), leaf CAB concentration, CC, and SL.

where $R_{measured}$ is a measured reflectance at wavelength λ and $R_{modeled}$ is a modeled reflectance at wavelength λ in the LUT, and n is the number of wavelengths.

LUT inversion was performed using extracted plot reflectance from Landsat and AVIRIS data and corresponding LUTs. For AVIRIS data, the inversion was carried out using full spectrum (184 bands) and 6 narrow AVIRIS bands having band centers closest to Landsat bands. The solution to the inverse problem was the set of input parameters corresponding to the reflectance in the database that provided the smallest RMSE. Because of the potential insufficiency in model formulation and parameterization, and noise related to calibration and pre-processing errors in the observed reflectance, the least RMSE solution might not necessarily provide the best estimates of LAI [43]. For this reason, for each observed spectrum, a range of closest matching spectra (10–250) were selected from the LUT. From the available multiple solutions (q), we chose the median LAI value among the multiple solutions as a final solution. Finally, we resampled LUTs of different dimensions to understand the effect of the LUT size on the accuracy of LAI retrieval. This was achieved by reducing the number of cases for input parameters individually in the best performing LUT followed by model inversion.

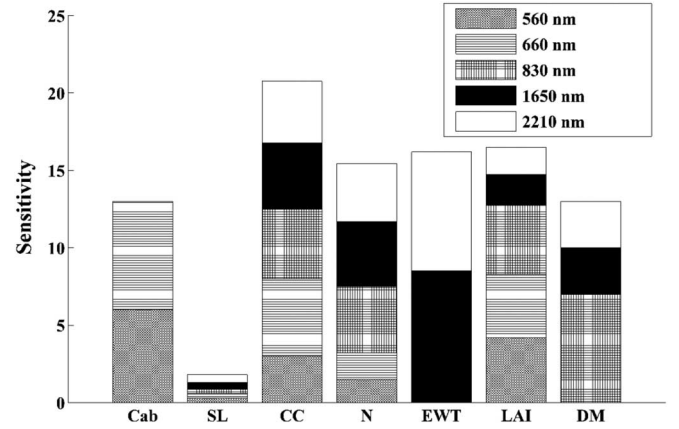


Fig. 3. Results of the SA in five Landsat TM bands: 560, 660, 830, 1650, and 2210 nm. The parameters are SL, Cab, CC, leaf structure parameter (N), leaf EWT, LAI, and leaf DM. Sensitivity refers to the relative importance of the parameters on the canopy reflectance. Each parameter was perturbed (varied) in turn keeping all other model parameters fixed at their reference values (base case). Sensitivity was calculated using perturbed and base reflectance at four bands for each parameter.

III. RESULTS

A. Parameter Combinations and SA

A preliminary LUT was generated with coarse increment levels for DART and PROSPECT parameters. The resulting table was searched for simulations that were comparable to the Landsat reflectance. Of a total of 762 048 preliminary simulations, only 62 757 (candidate simulations) were found to be within the space bounded by the image spectra (max/min space). In candidate solutions, earlier ranges for all parameters were unchanged.

The results of the SA are summarized in Fig. 3. Only two visible bands are shown in the diagram as the result was similar across other visible bands. The vertical height of each colored bar represents a sensitivity value, which is a measure of the relative importance of each parameter for causing variations in reflectance across five bands. The critical parameters found in our SA are as follows:

- 1) CC, Cab, and LAI in the visible band (560 and 660 nm);
- 2) CC, DM, N, and LAI in the near-infrared band (830 nm);
- 3) CC, EWT, and DM in the middle infrared band (1650 nm); and
- 4) EWT and DM in the shortwave infrared band (2210 nm).

The corresponding magnitudes of the greatest sensitivities were used to decide the maximum number of parameter cases for final simulation. This resulted in four, ten, eight, seven, and four cases for CC, EWT, DM, Cab, and N, respectively. A larger number of cases (25 with increment = 0.25) were assigned to LAI than indicated by the SA in order to increase its retrieval precision. A fixed value for SL (20%) was used because of its minimal influence on reflectance across the bands. The observed low sensitivity for SL was likely caused by the high values for crown cover (80%) and LAI (4) used in the SA. Fig. 4 shows the effects of four different LADs on reflectance over five broad bands. Plagiophile and extremophile LADs had similar

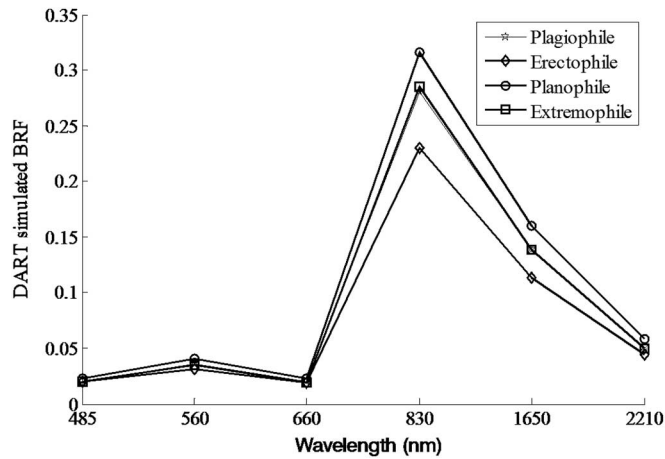


Fig. 4. Effect of four different LADs on DART-simulated BRF over six Landsat bands at LAI = 4, CC = 85%, leaf DM = (0.01 g/cm⁻²), leaf EWT = 0.01 cm, and Cab = 50 μg/cm⁻².

TABLE III
INPUT RANGES AND NUMBER OF CASES FOR FINAL SIMULATIONS

Parameters	Minimum	Maximum	Increment	No of cases
LAI (m ² /m ²)	1	7	0.25	25
EWT (cm)	0.001	0.019	0.002	10
DW (g/cm ⁻²)	0.001	0.022	0.003	8
N	1.5	3.5	0.5	4
Cab (μg/cm ⁻²)	10	80	11.6	7
CC (%)	50	100	16	4
LAD			—	3

The parameters are LAI, leaf EWT, leaf DM, leaf structural parameter (N), leaf CAB concentration, CC, and LAD. The three LADs used were erectophile, planophile, and plagiophile distributions.

effects on the reflectance. Hence, three LADs (planophile, plagiophile, and erectophile) were used in the final simulations.

Table III shows the free parameters, their ranges, increment, and the number of cases used for final simulations. If we had considered all the parameter combinations, 672 000 (25 * 10 * 8 * 7 * 4 * 4 * 3) simulations for each AVIRIS and Landsat band would have been required. After searching for realistic parameter combinations as illustrated in Appendix II, the total number of final simulations was reduced to 111 500.

B. Inversion

The final results from the LUT inversion are summarized in Table IV. The first column of the table shows the number of solutions considered. The other columns show the RMSE and R² between measured LAI and estimated LAI from the full spectrum of 184 narrow AVIRIS bands, 6 Landsat broad bands, and 6 narrow AVIRIS bands.

The results show that the LAI estimated from the full spectrum of AVIRIS bands (RMSE = 0.5) provided better accuracy (indicated by the lowest RMSE) than the LAI estimated from the Landsat (RMSE = 0.63) and six narrow AVIRIS bands

TABLE IV
RESULTS FROM THE LUT INVERSION

Number of solutions (q)	Median solution (AVIRIS all bands)		Median solution (Landsat)		Median solution (AVIRIS six bands)	
	RMSE	R ²	RMSE	R ²	RMSE	R ²
10	0.76	0.51	0.98	0.57	0.95	0.40
50	0.61	0.59	0.76	0.66	0.74	0.64
100	0.59	0.57	0.68	0.65	0.84	0.28
150	0.5	0.6	0.66	0.63	0.83	0.27
200	0.52	0.56	0.63	0.65	0.83	0.30
250	0.53	0.54	0.63	0.65	0.82	0.40

The first column shows the number of solutions selected for the least RMSE. The second, fourth, and sixth show the RMSE, and third, fifth, and seventh columns show the R² for inverted LAI using all AVIRIS bands, Landsat bands, and six narrow AVIRIS bands, respectively.

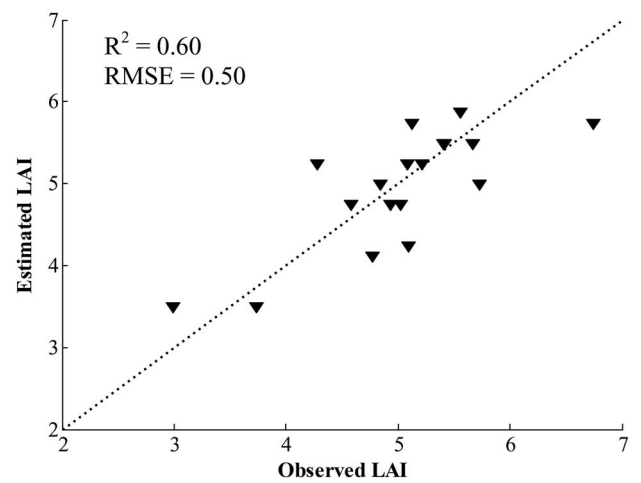


Fig. 5. Observed versus estimated LAI from full spectrum of AVIRIS bands using median value from 150 solutions. R² and RMSE refer to the square of the correlation coefficient and RMSE between observed and estimated LAI.

(RMSE = 0.74). With respect to the number of solutions (q), the median calculated from $q = 150$ provided the lowest RMSE for the full spectrum of AVIRIS bands, whereas the median calculated from $q = 200$ and $q = 50$ provided the lowest RMSE for Landsat and six narrow AVIRIS bands, respectively. The observed versus best-estimated LAI for individual inversion is shown in Figs. 5–7, and the boxplot of solutions are shown in Figs. 8–10. With only 17 plots used by Banskota *et al.* [49], the RMSE improved from 0.50 to 0.46 for full AVIRIS bands, from 0.63 to 0.61 for Landsat bands, and from 0.74 to 0.71 for six narrow AVIRIS bands (results not shown here). The effect of the LUT size on the LAI retrieval accuracy was tested with the best performing dataset, i.e., full spectrum AVIRIS. The results are summarized in Table V showing the original and altered cases of individual variables, total number of simulations, and the R² and RMSE between the observed and estimated LAI based on corresponding LUTs. The results show that the LUT of size (66 900 rows) created by removing simulations for three Cab cases (i.e., 20, 40, and 50 μg/cm²) showed improvement in RMSE (i.e., from 0.50 to 0.46); for all other instances, RMSE increased.

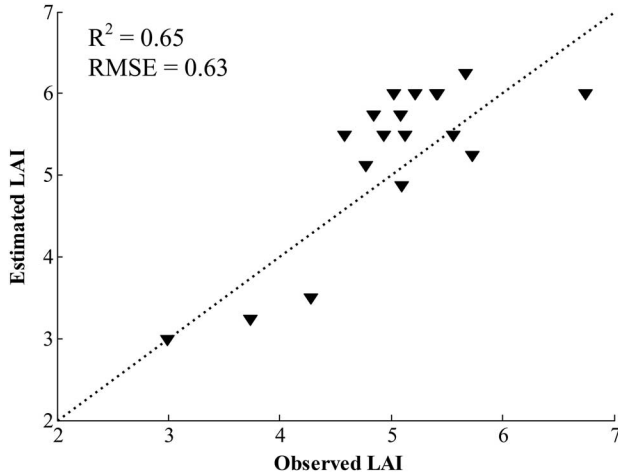


Fig. 6. Observed versus estimated LAI from Landsat data using median value from 250 solutions. R^2 and RMSE refer to the square of the correlation coefficient and RMSE between observed and estimated LAI.

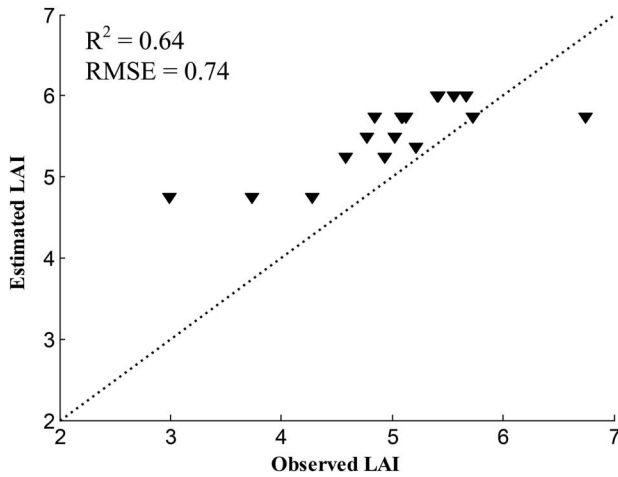


Fig. 7. Observed versus estimated LAI from 6 narrow AVIRIS bands using median value from 50 solutions. R^2 and RMSE refer to the square of the correlation coefficient and RMSE between observed and estimated LAI.

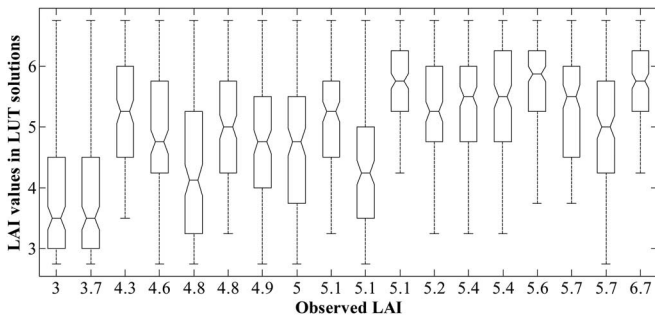


Fig. 8. Boxplots of LUT LAI values in 150 best matching spectra based on inversion using 184 narrow AVIRIS bands. The observed LAI values associated with boxplots are shown in X-axis.

IV. DISCUSSIONS

In this study, we used an LUT-based inversion of DART-simulated reflectances using AVIRIS and Landsat data to retrieve forest LAI. We determined the optimal parameter combinations and input increments for LUT creation, enabling

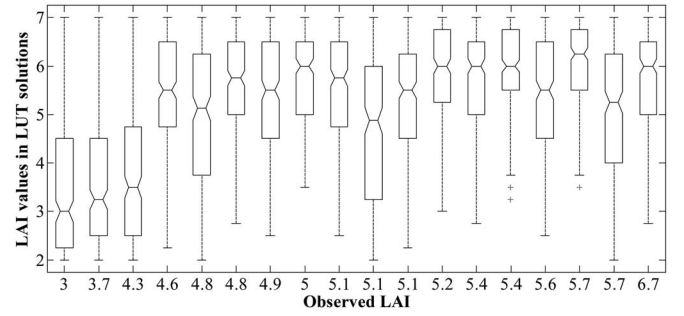


Fig. 9. Boxplots of LUT LAI values in 250 best matching spectra based on inversion using 6 broad Landsat bands. The observed LAI values associated with boxplots are shown in X-axis.

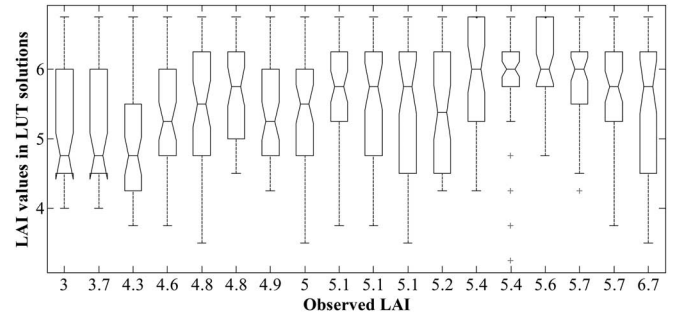


Fig. 10. Boxplots of LUT LAI values in 50 best matching spectra based on inversion using 6 narrow AVIRIS bands. The observed LAI values associated with boxplots are shown in X-axis.

TABLE V
 R^2 AND RMSE BETWEEN OBSERVED AND ESTIMATED LAI FOR DIFFERENT LUT SIZE

Variables	Cases (original)	Cases (altered)	LUT size	R^2	RMSE
Cab	7	4	66 900	0.68	0.46
Cab	7	3	44 600	0.53	0.57
EWT	10	5	63 000	0.58	0.53
DW	8	4	53 390	0.49	0.58
LAD	3	2	64 690	0.46	0.62
CC	4	2	75 050	0.53	0.6

The different LUT size was achieved by altering the number of cases for individual variables.

DART to simulate reflectance spectra commensurate to those measured by the Landsat and AVIRIS sensors. The inversion resulted in reasonably accurate LAI estimates (RMSE = 0.50 with AVIRIS and 0.64 with Landsat). Typical DART simulations to create LUT for inversion require significant computational resources [27]. Furthermore, high-dimensional image data, such as AVIRIS, increase computational time given the large number of spectral channels. Demarez and Gastellu-Etchegorry [59] tested an interpolation technique for precomputed canopy reflectance values simulated through the coupling of DART and PROSPECT. Kimes *et al.* [20] also employed a similar interpolation procedure to produce directional reflectance values to estimate forest characteristics. Such interpolation procedures significantly reduce the number of simulations necessary, but still require a large number of simulations to accurately interpolate reflectance when many model

inputs have unknown values or ranges. Additional studies have devised automated forward modeling parameterization techniques to build LUTs for improved inversion [39], [47], [48]. However, such techniques require a model to be run in multiple forward modes, which is not computationally feasible for DART. The results of this study show that the outlined three-step approach can be helpful for building an LUT of optimal size for accurate LAI estimation, which can be scaled up for larger problems covering broader regions.

The results indicate that the approach can be used to identify the realistic range for an individual parameter as suggested by Peddle *et al.* [48]. Moreover, the results show that not all possible combinations within the identified range provide output similar to the image reflectance, and leaving out such infeasible combinations with a simple search process results in significantly less computation time. Such efficiency may be increased by further incorporating information on observed trait variation (e.g., [50]) when developing the LUT ranges and parameter distributions [64]. In this study, it required 840 h to compute reflectance for the final 115 000 simulations for AVIRIS bands using a computer with 32 processors and 64 GB of physical RAM. If we had considered all possible combinations (779 520 simulations), it would have taken nearly seven times longer. It is also likely that considering all the possible combinations would not have provided any significant improvements in the estimation of LAI, given that many of the simulations would have fallen outside of the range in image spectra (e.g., [64]). Present DART 5.5.1 version, which is multithreaded and optimizes the computation of ray paths, is much faster for conducting hyperspectral simulations than the DART version that we used here.

Our previous work (Banskota *et al.* [49]) used a similar approach for constraining the LUT grid size and resolution based on image information. But in that study, we used plot spectra to limit the parameter range and combinations. Such strategy reduces the required number of simulations, but unrealistically makes an assumption that all image spectra of vegetation types in question are bound by the plot spectral range, which would therefore require a large number of sample plots to constrain the LUT for broad regions. In this study, we used atmospherically corrected and cloud-masked near-anniversary Landsat reflectance product and land cover data to determine the range of image reflectance. This approach required a larger number of simulations (115 000) relative to that used by Banskota *et al.* [49] (28 000) for the same set of AVIRIS and plot dataset, but ensured that the spatial variation in the band reflectance was sufficiently captured. Fewer simulations might have been required, had we used AVIRIS image in lieu of Landsat to constrain the LUT; however, our approach allowed us to compare the inversion results from both sensors.

Our results presented here show that the inversion using all available AVIRIS bands provided better LAI estimates than the inversion using Landsat broad bands. This shows that the greater information content in a larger number of narrow spectral bands in a spectroscopic data is likely beneficial for improved LAI retrieval from remote sensing data. On the contrary, Weiss *et al.* [43] reported that only a limited number of wavebands are required for canopy biophysical variable

estimation. This is especially true for hyperspectral data with noisy or poorly modeled wavebands by the RTM being inverted [65]. Other studies have indicated that the selection of a subset of spectral bands—or alternatively the weighting of different spectral bands—can lead to a more stable and accurate inversion [3], [38], [45]. In this study, we selected six narrow bands with closest band center to the Landsat bands and carried out the inversion based on the subset of bands. The results obtained were, however, poorer than those obtained by Landsat broad bands. This may have been related to atmospheric correction artifacts where the AVIRIS image spectra were not adequately described by the atmospheric algorithm (in this case, ACORN) resulting in a biased comparison. The potential bias is evident in Fig. 7 where most observations systematically fell above the 1:1 line in the observed versus estimated plot. On the other hand, the median retrieval using the full spectrum of bands might have accounted for the potential bias by enabling less strict requirements on the modeled and observed reflectance comparison.

According to Weiss *et al.* [43], the best parameter retrieval is achieved when the number of solutions (q) ranges between 10 and 50. Darvishzadeh *et al.* [66] did not find any significant difference in the results obtained from $q = 10$ and 100 cases, whereas Darvishzadeh *et al.* [67] found the best solution when $q = 250$ cases. In this study, we observed the best LAI estimate with $q = 150$. Such differences in the appropriate number of solutions are potentially caused by the size and density of the LUT grid and the noise in the modeled and observed reflectance [43], [67]. Nevertheless, RMSE decreases when $q > 10$ and converges and becomes stable when q approaches 150 as observed in this study as well as by Darvishzadeh *et al.* [67]. Hence, multiple solutions with $q > 100$ seems necessary to achieve near optimum, if not the best, solution. For six narrow bands, the RMSE did not improve with an increase in the number of solutions beyond $q = 50$. The comparison between AVIRIS image spectra and the simulations in the multiple solutions revealed that greater mismatch occurred in the visible bands, where the AVIRIS reflectance was lower than simulations potentially due to overcompensation of atmospheric effects. The effect of atmospheric correction artifact was much pronounced when inverted using six narrow bands due to equal weight given to visible and infrared bands (three each) compared to full spectrum (many infrared than visible bands). When $q = 50$, as seen in Fig. 7, the effect of the low-visible reflectance resulted in overestimation mainly at lower LAI values. With $q \geq 100$, the overestimation occurred even at higher LAI values (figures for higher number of solutions not shown here). The plot LAI was estimated using digital hemispherical photography processed with DHP [5], following the protocol of Zhang *et al.* [54] for increasing the contrast between foliage and sky. We acknowledge that LAI measurement uncertainty is an important consideration in remote sensing research as any optical (e.g., DHP), active (e.g., Lidar), or direct measurement (e.g., litter traps and destructive harvesting) can only provide estimates of true stand-level LAI [43], [51]. The uncertainty in ground measured LAI is a result of the assumptions that are required for the various techniques (e.g., assumptions related to crown geometry, foliar distribution, LAD, seasonal

leaf replacement or exchange, leaf optical properties, etc.) and the accuracies of measurement protocols (e.g., gap fraction, individual leaf area/mass, spatial sampling, etc.) as well as other factors that are more difficult to quantify over large areas (e.g., shoot and canopy clumping). However, given all the issues with indirect quantification of LAI, it has been well established that the properties related to clumping (at the shoot and canopy scales) are those that dominate the uncertainties [51]. Some studies have shown reasonable agreement between DHP and traditional allometric and destructive estimates (e.g., [51], [63]) when properly accounting for foliage clumping. We recognize that the estimation of the degree of foliage clumping with DHP-TRAC software in this study might not provide sufficient quantification of clumping at our sites and potentially contributed to the overall retrieval uncertainty; however, Leblanc *et al.* [5] and Chen *et al.* [1] generally showed close agreement between the methods.

SA could help identify both the inconsequential parameters and the number of cases for each input parameter in the final simulation. If a parameter has low sensitivity to canopy spectral reflectance changes, it should be excluded from the inversion and kept at a realistic fixed value [45]. If the parameter has high sensitivity, it should be densely represented in the LUT. Hence, an ideal implementation of an LUT would comprise an adaptive grid where the numbers of cases of model parameters are guided by their respective sensitivity to the changes in spectral reflectance. In this study, we utilized a simple SA where the variations for individual parameters were considered independently. The inversion results using smaller size LUT indicated that further reduction in parameter cases than guided by the SA is possible. The retrieval accuracy slightly improved for reduced-size LUT created by fewer Cab cases. LAI and leaf chlorophyll values generally tend to correlate; however, such interaction between parameter was not analyzed in the SA. There are other methods, such as the extended Fourier amplitude sensitivity test (EFAST), which provides information on the effect of interactions among variables in model output [68]. Such methods, however, require a significantly greater number of simulations than required by the simple method used in this study.

V. CONCLUSION

We devised an efficient way of building LUT for the inversion of the DART model using hyperspectral remote sensing data. We used an approach for selecting realistic parameter combinations based on the information derived from the Landsat image. The approach used a coarse-resolution LUT built for broad Landsat bands to determine the optimal parameterization space that is likely to simulate canopy reflectance similar to that recorded by remote sensing measurements. A sensitivity study determined the optimal input increments. The improved LAI estimates obtained by the inversion of the DART model based on AVIRIS data than Landsat data suggested that the approach might be helpful for an efficient building of LUT for hyperspectral bands. The study, however, employed few simplifications in DART parameterization (e.g., constant fraction of diffuse radiation, absence of ground vegetation, constant

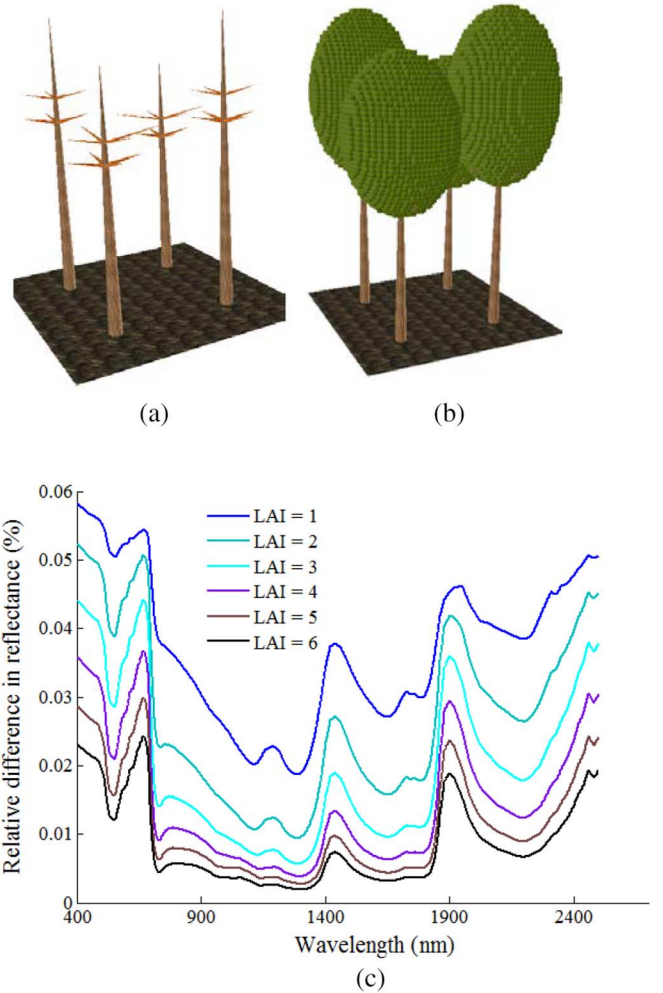


Fig. 11. Impact of the branches on nadir reflectance of a tree cover (80%) with LAI from 1 to 6 when Sun zenith angle is 27° . (a) Four-tree scene where trees are simulated with schematic branches, for the case “LAI = 0.” (b) Four-tree scene where trees are simulated with foliage, and with and without schematic branches. (c) Relative difference of the reflectance of a “4-tree” scene with and without schematic branches.

SL, etc.) and tested the LUT inversion using plots spectra with high LAI values (≥ 3). We recommend that the future studies take into account of the spectral variation in sky irradiance and background reflectance. With the new multithreaded DART, simulations can be conducted with more realistic conditions such as actual atmosphere spectral illumination, trees with branches, variable SL with less computational cost than that required by the DART version used in this study. Further study needs to be done in regions with greater dynamic range of LAI and prominent ground vegetation to confirm the broader applicability of the approach.

APPENDIX I

DART SIMULATION WITH AND WITHOUT BRANCHES

We assessed the difference in the DART-simulated reflectance using trees described with and without schematic branches. Fig. 11(a) shows a four-tree scene where trees are simulated with schematic branches, for the case “LAI = 0,”

TABLE VI
(APPENDIX II) ONE OF THE RESULTS FROM SEARCH FOR REALISTIC COMBINATIONS
OF PARAMETERS

CC (%)	DM (g/cm ⁻²)	EWT (cm)	LAI (m ² /m ²)	LAD	Cab (μg/cm ⁻²)
		0.001	–	–	–
		0.004	3–6	[2]	10–30
		0.007	2–6	[2, 4, 5]	10–50
	0.001	0.01	1–6	[2, 3, 4, 5]	10–80
		0.013	1–6	[2, 3, 4, 5]	10–80
		0.016	1–6	[2, 3, 4, 5]	10–80
		0.019	1–6	[2, 3, 4, 5]	10–80
		0.001	1–6	[2, 3, 4, 5]	10–80
		0.004	1–6	[2, 3, 4, 5]	10–80
100	0.01	0.007	1–6	[2, 3, 4, 5]	30–80
		0.01	1–6	[3, 4, 5]	30–60
		0.013	1–6	[3, 4, 5]	30–80
		0.016	1–6	[3]	30–80
		0.019	1–6	[3]	30–80
		0.001	1–6	[2, 3, 4, 5]	10–80
		0.004	1–6	[2, 3, 4, 5]	10–80
	0.021	0.007	1–6	[3, 4, 5]	20–80
		0.01	2–5	[3]	30–60
		0.013	–	–	–

The parameters are CC, Leaf DM, Leaf EWT, LAI, LAD, and Leaf CAB Concentration. The four LADs were erectophile (2), planophile (3), extremophile (4), and plagiophile (5) distributions.

and Fig. 11(b) shows the four-tree scene with foliage, with and without schematic branches. The relative difference in reflectance between scenes where the crowns are simulated with and without branches is plotted in Fig. 11(c). The figure shows that the relative difference in reflectance (in y-axis) is generally smaller than 1% with LAI around 4. As expected, this relative difference inversely varies with LAI: it increases with smaller LAI and decreases with larger LAI.

APPENDIX II ITERATIVE SEARCHING FOR BEST PARAMETER COMBINATIONS

Model inputs that led to simulations (candidate solutions) in the reduced LUT were examined to infer information about optimal ranges and parameter combinations. As shown in Fig. 2, the useful parameter combinations that produce reflectance values within the range of image spectra were searched with the following iterative steps. First, start searching candidate simulations for a single value of CC (e.g., CC = 100%) and create a reduced-size table with only those simulations (LUT1). Then, take a single DM (e.g., DM = 0.01 g/cm²) present in LUT1 and create another reduced-size table (LUT2). From LUT2, create LUT3 for one of the values of EWT. Query a range of values for the remaining parameters (Cab, LAI, LAD, and N) in LUT3 and make a list of them. Repeat the process for all remaining values of EWT in LUT3,

followed by the rest of the values of DM in LUT2 and finally all values of CC in LUT1.

The results of the above search process were listed as optimal input ranges for four parameters for each combination of CC, DM, and EWT present in candidate solutions. In principle, the process could be repeated for all combinations of parameters, but it would have returned an overly large set of results that would be difficult to interpret. We considered CC, DM, and EWT in the search process as their unique values had significantly different frequencies in candidate solutions. All parameter values for N and SL, in contrast, were represented in about equal proportion in candidate solutions. The results would have been similar for all combinations of their values, and would not have revealed much information about optimal parameter combinations.

One of the results of the search for optimal parameter combinations is shown in Table VI. The table shows all parameter combinations in candidate simulations with 100% CC and three DM values that produced reflectance within the max/min space. None of the simulations for two parameter combinations (EWT = 0.001 cm and DM = 0.001 g/cm⁻²; and EWT > 0.013 and DM = 0.021 g/cm²) was selected. This showed that any combinations of DM greater than or equal to 0.021 g/cm² with 100% CC and 0.016 cm EWT were less likely to result in reflectance similar to that of image and could be discarded at the final LUT building process. Similarly, only LAI values between 2 and 5 combined with 0.01 cm EWT, 0.021 g/cm² DM, and 100% CC resulted in candidate solutions. This suggested that

we could leave out LAI values greater than or equal to 6 for the particular parameters combination.

ACKNOWLEDGMENT

The authors would like to thank the anonymous reviewers for thorough review and providing useful comments and edits.

REFERENCES

- [1] J. M. Chen *et al.*, "Leaf area index measurements at Fluxnet-Canada forest sites," *Agric. For. Meteorol.*, vol. 140, pp. 257–268, 2006.
- [2] K. F. Huemmrich, J. L. Privette, M. Mukelabai, R. B. Myneni, and Y. Knyazikhin, "Time-series validation of MODIS land biophysical products in a Kalahari woodland, Africa," *Int. J. Remote Sens.*, vol. 26, pp. 4381–4398, 2005.
- [3] M. Meroni, R. Colombo, and C. Panigada, "Inversion of a radiative transfer model with hyperspectral observations for LAI mapping in poplar plantations," *Remote Sens. Environ.*, vol. 92, pp. 195–206, 2004.
- [4] R. B. Myneni *et al.*, "Global products of vegetation leaf area and fraction absorbed PAR from year one of MODIS data," *Remote Sens. Environ.*, vol. 83, pp. 214–231, 2002.
- [5] S. G. Leblanc, J. M. Chen, R. Fernandes, D. W. Deering, and A. Conley, "Methodology comparison for canopy structure parameters extraction from digital hemispherical photography in boreal forests," *Agric. For. Meteorol.*, vol. 129, pp. 187–207, 2005.
- [6] Z. Malenovsky *et al.*, "Influence of woody elements of a Norway spruce canopy on nadir reflectance simulated by the DART model at very high spatial resolution," *Remote Sens. Environ.*, vol. 112, pp. 1–18, 2008.
- [7] G. P. Asner, "Biophysical and biochemical sources of variability in canopy reflectance," *Remote Sens. Environ.*, vol. 64, pp. 234–253, 1998.
- [8] B. Koetz, F. Baret, H. Poilvé, and J. Hill, "Use of coupled canopy structure dynamic and radiative transfer models to estimate biophysical canopy characteristics," *Remote Sens. Environ.*, vol. 95, pp. 115–124, 2005.
- [9] K. S. Fassnacht, S. T. Gower, M. D. MacKenzie, E. V. Nordheim, and T. M. Lillesand, "Estimating the leaf area index of north central Wisconsin forest using the Landsat Thematic Mapper," *Remote Sens. Environ.*, vol. 61, pp. 229–245, 1997.
- [10] P. Gong, R. L. Pu, and J. R. Miller, "Coniferous forest leaf-area index estimation along the Oregon transect using compact airborne spectrographic imager data," *Photogramm. Eng. Remote Sens.*, vol. 61, pp. 1107–1117, 1995.
- [11] P. M. Hansen and J. K. Schjoerring, "Reflectance measurement of canopy biomass and nitrogen status in wheat crops using normalized difference vegetation indices and partial least squares regression," *Remote Sens. Environ.*, vol. 86, pp. 542–553, 2003.
- [12] K. F. Huemmrich, J. L. Privette, M. Mukelabai, R. B. Myneni, and Y. Knyazikhin, "Time-series validation of MODIS land biophysical products in a Kalahari woodland, Africa," *Int. J. Remote Sens.*, vol. 26, pp. 4381–4398, 2005.
- [13] M. E. Schaepman, B. Koetz, G. Schaepman-Strub, and K. I. Itten, "Spectrodirectional remote sensing for the improved estimation of biophysical and -chemical variables: Two case studies," *Int. J. Appl. Earth Observ. Geoinf.*, vol. 6, pp. 271–282, 2005.
- [14] A. Banskota *et al.*, "Investigating the utility of the wavelet transform for temperate forest LAI estimation using hyperspectral data," *Photogramm. Eng. Remote Sens.*, vol. 79, pp. 653–662, 2013.
- [15] Q. Xie *et al.*, "Leaf area index estimation using vegetation indices derived from airborne hyperspectral images in winter wheat," *IEEE J. Sel. Topics Appl. Earth Observ. Remote Sens.*, vol. 7, no. 8, pp. 3586–3594, Aug. 2014.
- [16] J. P. R. Caicedo, J. Verrelst, J. Munoz-Mari, J. Moreno, and G. Camps-Valls, "Toward a semiautomatic machine learning retrieval of biophysical parameters," *IEEE J. Sel. Topics Appl. Earth Observ. Remote Sens.*, vol. 7, no. 4, pp. 1249–1259, Apr. 2014.
- [17] N. Gobron, B. Pinty, and M. M. Verstraete, "Theoretical limits to the estimation of the leaf area index on the basis of visible and near-infrared remote sensing data," *IEEE Trans. Geosci. Remote Sens.*, vol. 35, no. 6, pp. 1438–1445, Nov. 1997.
- [18] P. J. Curran, "Imaging spectrometry," *Prog. Phys. Geogr.*, vol. 18, pp. 247–266, 1994.
- [19] D. R. Peddle *et al.*, "Applications of the BIOPHYS algorithm for physically-based retrieval of biophysical, structural and forest disturbance information," *IEEE J. Sel. Topics Appl. Earth Observ. Remote Sens.*, vol. 4, no. 4, pp. 971–982, Dec. 2011.
- [20] D. Kimes, Y. Knjazikhin, J. Privette, A. Abuelgasim, and F. Gao, "Inversion methods for physically based models," *Remote Sens. Rev.*, vol. 18, pp. 381–439, 2000.
- [21] M. M. Verstraete, B. Pinty, and R. B. Myneni, "Potential and limitations of information extraction on the terrestrial biosphere from satellite remote sensing," *Remote Sens. Environ.*, vol. 58, pp. 201–214, 1996.
- [22] K. Richter, C. Atzberger, F. Vuolo, and G. D'Urso, "Evaluation of Sentinel-2 spectral sampling for radiative transfer model based LAI estimation of wheat, sugar beet, and maize," *IEEE J. Sel. Topics Appl. Earth Observ. Remote Sens.*, vol. 4, no. 2, pp. 458–464, Jun. 2011.
- [23] M. Yebra and E. Chuvieco, "Generation of a species-specific look-up table for fuel moisture content assessment," *IEEE J. Sel. Topics Appl. Earth Observ. Remote Sens.*, vol. 2, no. 1, pp. 21–26, Mar. 2009.
- [24] M. Chopping *et al.*, "Large area mapping of southwestern forest crown cover, canopy height, and biomass using the NASA multiangle imaging spectro-radiometer," *Remote Sens. Environ.*, vol. 112, pp. 2051–2063, 2008.
- [25] R. Darvishzadeh, A. Skidmore, M. Schlerf, and C. Atzberger, "Inversion of a radiative transfer model for estimating vegetation LAI and chlorophyll in heterogeneous grassland," *Remote Sens. Environ.*, vol. 112, pp. 2592–2604, 2008.
- [26] J. P. Gastellu-Etchegorry, V. Demarez, V. Pinel, and F. Zagolski, "Modeling radiative transfer in heterogeneous 3-D vegetation canopies," *Remote Sens. Environ.*, vol. 58, pp. 131–156, 1996.
- [27] J. P. Gastellu-Etchegorry, F. Gascon, and P. Esteve, "An interpolation procedure for generalizing a look-up table inversion method," *Remote Sens. Environ.*, vol. 87, pp. 55–71, 2003.
- [28] R. B. Myneni, "Modeling radiative transfer and photosynthesis in three dimensional vegetation canopies," *Agric. For. Meteorol.*, vol. 55, pp. 323–344, 1991.
- [29] R. B. Myneni, G. Asrar, and F. G. Hall, "A three-dimensional radiative transfer method for optical remote sensing of vegetated land surfaces," *Remote Sens. Environ.*, vol. 41, pp. 105–121, 1992.
- [30] L. Xiaowen and A. H. Strahler, "Geometric-optical modeling of a conifer forest canopy," *IEEE Trans. Geosci. Remote Sens.*, vol. GE-23, no. 5, pp. 705–721, Sep. 1985.
- [31] S. G. Leblanc and J. M. Chen, "A windows graphic user interface (GUI) for the five-scale model for fast BRDF simulations," *Remote Sens. Rev.*, vol. 19, pp. 293–305, 2001.
- [32] F. Gascon, J. P. Gastellu-Etchegorry, M. J. Lefevre-Fonollosa, and E. Dufrene, "Retrieval of forest biophysical variables by inverting a 3-D radiative transfer model and using high and very high resolution imagery," *Int. J. Remote Sens.*, vol. 25, pp. 5601–5616, 2004.
- [33] J. P. Gastellu-Etchegorry, E. Martin, and F. Gascon, "DART: A 3D model for simulating satellite images and studying surface radiation budget," *Int. J. Remote Sens.*, vol. 25, pp. 73–96, 2004.
- [34] S. Duthoit, V. Demarez, J. P. Gastellu-Etchegorry, E. Martin, and J. L. Roujean, "Assessing the effects of the clumping phenomenon on BRDF of a maize crop based on 3D numerical scenes using DART model," *Agric. For. Meteorol.*, vol. 148, pp. 1341–1352, 2008.
- [35] B. Pinty *et al.*, "Radiation transfer model intercomparison (RAMI) exercise: Results from the second phase," *J. Geophys. Res. Atmos.*, vol. 109, p. 19, 2004.
- [36] D. S. Kimes, R. F. Nelson, M. T. Manry, and A. K. Fung, "Attributes of neural networks for extracting continuous vegetation variables from optical and radar measurements," *Int. J. Remote Sens.*, vol. 19, pp. 2639–2663, 1998.
- [37] D. Kimes, J. Gastellu-Etchegorry, and P. Estève, "Recovery of forest canopy characteristics through inversion of a complex 3D model," *Remote Sens. Environ.*, vol. 79, pp. 320–328, 2002.
- [38] M. Schlerf and C. Atzberger, "Inversion of a forest reflectance model to estimate structural canopy variables from hyperspectral remote sensing data," *Remote Sens. Environ.*, vol. 100, pp. 281–294, 2006.
- [39] J. Hedley, C. Roelfsema, and S. R. Phinn, "Efficient radiative transfer model inversion for remote sensing applications," *Remote Sens. Environ.*, vol. 113, pp. 2527–2532, 2009.
- [40] S. Liang, "Recent developments in estimating land surface biogeophysical variables from optical remote sensing," *Prog. Phys. Geogr.*, vol. 31, pp. 501–516, 2007.
- [41] Y. Knyazikhin, J. Martonchik, R. Myneni, D. Diner, and S. Running, "Synergistic algorithm for estimating vegetation canopy leaf area index and fraction of absorbed photosynthetically active radiation from MODIS and MISR data," *J. Geophys. Res.*, vol. 103, pp. 32257–32276, 1998.

- [42] K. Omari, H. P. White, K. Staenz, and D. J. King, "Retrieval of forest canopy parameters by inversion of the PROFILAIR leaf-canopy reflectance model using the LUT approach," *IEEE J. Sel. Topics Appl. Earth Observ. Remote Sens.*, vol. 6, no. 2, pp. 715–723, Apr. 2013.
- [43] M. Weiss, F. Baret, R. B. Myneni, A. Pragnere, and Y. Knyazikhin, "Investigation of a model inversion technique to estimate canopy biophysical variables from spectral and directional reflectance data," *Agronomie*, vol. 20, pp. 3–22, 2000.
- [44] C. D. Mobley *et al.*, "Interpretation of hyperspectral remote-sensing imagery by spectrum matching and look-up tables," *Appl. Opt.*, vol. 44, pp. 3576–3592, 2005.
- [45] M. J. Barnsley *et al.*, "On the potential of CHRIS/PROBA for estimating vegetation canopy properties from space," *Remote Sens. Rev.*, vol. 19, pp. 171–189, 2000.
- [46] B. Combal *et al.*, "Retrieval of canopy biophysical variables from bidirectional reflectance: Using prior information to solve the ill-posed inverse problem," *Remote Sens. Environ.*, vol. 84, pp. 1–15, 2002.
- [47] D. R. Peddle, S. E. Franklin, R. L. Johnson, M. A. Lavigne, and M. A. Wulder, "Structural change detection in a disturbed conifer forest using a geometric optical reflectance model in multiple-forward mode," *IEEE Trans. Geosci. Remote Sens.*, vol. 41, no. 1, pp. 163–166, Jan. 2003.
- [48] D. R. Peddle *et al.*, "Physically-based inversion modeling for unsupervised cluster labeling, independent forest classification and LAI estimation using MFM-5-scale," *Can. J. Remote Sens.*, vol. 33, pp. 214–225, 2007.
- [49] A. Banskota *et al.*, "Investigating the utility of wavelet transforms for inverting a 3-D radiative transfer model using hyperspectral data to retrieve forest LA," *Remote Sens.*, vol. 5, pp. 2639–2659, 2013.
- [50] S. P. Serbin, A. Singh, B. E. Mcneil, C. C. Kingdon, and P. A. Townsend, "Spectroscopic determination of leaf morphological and biochemical traits for northern temperate and boreal tree species," *Ecol. Appl.*, vol. 24, pp. 1651–1669, 2014.
- [51] J. T. Curtis, *The Vegetation of Wisconsin: An Ordination of Plant Communities*, 2nd ed. Madison, WI, USA: Univ. of Wisconsin Press, 1959.
- [52] I. Jonckheere *et al.*, "Review of methods for in situ leaf area index determination—Part I. Theories, sensors and hemispherical photography," *Agric. For. Meteorol.*, vol. 121, pp. 19–35, 2004.
- [53] J. M. Chen *et al.*, "Leaf area index measurements at Fluxnet-Canada forest sites," *Agric. For. Meteorol.*, vol. 140, pp. 257–268, 2006.
- [54] Y. Q. Zhang, J. M. Chen, and J. R. Miller, "Determining digital hemispherical photograph exposure for leaf area index estimation," *Agric. For. Meteorol.*, vol. 133, pp. 166–181, 2005.
- [55] R. Fernandes, J. R. Miller, J. M. Chen, and I. G. Rubinstein, "Evaluating image-based estimates of leaf area index in boreal conifer stands over a range of scales using high-resolution CASI imagery," *Remote Sens. Environ.*, vol. 89, pp. 200–216, 2004.
- [56] S. G. Leblanc and J. M. Chen, "A practical scheme for correcting multiple scattering effects on optical LAI measurements," *Agric. For. Meteorol.*, vol. 110, pp. 125–139, 2001.
- [57] R. O. Green *et al.*, "Imaging spectroscopy and the airborne visible infrared imaging spectrometer (AVIRIS)," *Remote Sens. Environ.*, vol. 65, pp. 227–248, 1998.
- [58] J. G. Masek *et al.*, "A Landsat surface reflectance data set for North America, 1990–2000," *IEEE Geosci. Remote Sens. Lett.*, vol. 3, no. 1, pp. 68–72, Jan. 2006.
- [59] G. Chander, C. Huang, L. Yang, C. Homer, and C. Larson, "Developing consistent Landsat data sets for large area applications: The MRLC 2001 protocol," *IEEE Geosci. Remote Sens. Lett.*, vol. 6, no. 4, pp. 777–781, Oct. 2009.
- [60] M. Jacquemoud, "Inversion of the PROSPECT + SAIL canopy reflectance model from AVIRIS equivalent spectra: Theoretical study," *Remote Sens. Environ.*, vol. 44, pp. 281–292, 1993.
- [61] C. T. de Wit, *Photosynthesis of Leaf Canopies*. Wageningen, The Netherlands: Pudoc Publ., 1965.
- [62] A. d. Santis, E. Chuvieco, and P. J. Vaughan, "Short-term assessment of burn severity using the inversion of PROSPECT and GeoSail models," *Remote Sens. Environ.*, vol. 113, pp. 126–136, 2009.
- [63] J. L. Privette, R. B. Myneni, C. J. Tucker, and W. J. Emery, "Invertibility of a 1-D discrete ordinates canopy reflectance model," *Remote Sens. Environ.*, vol. 48, pp. 89–105, 1994.
- [64] J. B. Féret *et al.*, "Optimizing spectral indices and chemometric analysis of leaf chemical properties using radiative transfer modeling," *Remote Sens. Environ.*, vol. 115, pp. 2742–2750, 2011.
- [65] V. Demarez and J. P. Gastellu-Etchegorry, "A modeling approach for studying forest chlorophyll content," *Remote Sens. Environ.*, vol. 71, pp. 226–238, 2000.
- [66] R. Darvishzadeh, C. Atzberger, A. Skidmore, and M. Schlerf, "Mapping grassland leaf area index with airborne hyperspectral imagery: A comparison study of statistical approaches and inversion of radiative transfer models," *ISPRS J. Photogramm. Remote Sens.*, vol. 66, pp. 894–906, 2011.
- [67] R. Darvishzadeh, A. A. Matkan, and A. D. Ahangar, "Inversion of a radiative transfer model for estimation of rice canopy chlorophyll content using a lookup-table approach," *IEEE J. Sel. Topics Appl. Earth Observ. Remote Sens.*, vol. 5, no. 4, pp. 1222–1230, Aug. 2012.
- [68] A. Saltelli, S. Tarantola, and K. P. S. Chan, "A quantitative model-independent method for global sensitivity analysis of model output," *Technometrics*, vol. 41, pp. 39–56, 1999.
- [69] M. Rautiainen, "Retrieval of leaf area index for a coniferous forest by inverting a forest reflectance model," *Remote Sens. Environ.*, vol. 99, pp. 295–303, 2005.



Asim Banskota received the Bachelor's degree in environmental science from Kathmandu University, Dhulikhel, Nepal, in 2002, the Master's degree in geo-information science and earth observation from ITC, Enschede, the Netherlands, in 2007, and the Ph.D. degree in geospatial and environmental analysis, Virginia Polytechnic Institute and State University, Blacksburg, VA, USA, in 2011.

He is a Research Associate with the Department of Forest Resources, University of Minnesota, Minneapolis, MN, USA. He previously worked with the Center for Rural Technology, Nepal and Resources Himalaya Foundation, Nepal at different capacities before joining the Ph.D. program. He also worked with Conservation International, Arlington, VA, USA, as a Senior Remote Sensing Analyst and Research Assistant Professor with Michigan Technological University, Houghton, MI, USA, prior to his current position. His research interests include remote sensing applications to study vegetation condition and terrestrial ecosystem dynamics.



Shawn P. Serbin received the B.A. degree in telecommunications and GIS from Michigan State University, Houghton, MI, USA, in 2004, and the double M.Sc. degree in environmental monitoring and forestry and Ph.D. degree in forest ecology from the University of Wisconsin-Madison, Madison, WI, USA, in 2008 and 2012, respectively.

He is currently an Assistant Scientist with Brookhaven National Laboratory, Upton, NY, USA, and an Affiliate Faculty Member with the Department of Sustainability Studies, Stony Brook University, Stony Brook, NY, USA. He has been with Brookhaven National Laboratory since 2014 and was previously a Postdoctoral Research Associate with the Department of Forest and Wildlife Ecology, University of Wisconsin-Madison (2012–2014) and the Department of Plant Biology, University of Illinois at Urbana-Champaign, Champaign, IL, USA (2011–2012). His research interests include the use of remote sensing, particularly spectroscopy, and novel model-data synthesis approaches to scale process knowledge and study the exchanges of carbon, water and energy between terrestrial ecosystems and the atmosphere, especially in relation to natural and anthropogenic perturbations.



Randolph H. Wynne received the Ph.D. degree in environmental monitoring from the University of Wisconsin-Madison, Madison, WI, USA, in 1995.

He is currently a Professor with the Department of Forest Resources and Environmental Conservation, Virginia Polytechnic Institute and State University, Blacksburg, VA, USA, where he also serves as Co-Director of the Interdisciplinary Graduate Education Program in Remote Sensing and Co-Director of the Center for Environmental Applications of Remote Sensing, Blacksburg, VA, USA. He is a Member of the Landsat Science Team. His research interests include algorithm development, multitemporal analysis of forest disturbance and recovery, ecosystem service assessment and modeling, and terrestrial ecology.



Valerie A. Thomas received the B.Sc. (Eng.) degree in environmental engineering from the University of Guelph, Guelph, ON, Canada, in 1996, the Advanced Diploma degree in remote sensing from the College of Geographic Sciences, Lawrencetown, NS, Canada, in 1998, the M.Sc. and Ph.D. degrees in geography from Queen's University, Kingston, ON, Canada, in 2001 and 2006, respectively.

In 2006, she was a Postdoctoral Fellow for Fluxnet-Canada with the Department of Geography, Queen's University. She is currently an Associate Professor of Remote Sensing with the Department of Forest Resources and Environmental Conservation, Virginia Tech, Blacksburg, VA, USA. Her research interests include the use of remote sensing to examine forest canopy physiology, structure, and function across space and time.



Michael J. Falkowski received the Bachelor's degree in geography from the University of Wisconsin, Stevens Point, WI, USA, in 2000, and the M.S. and Ph.D. degrees in forestry and natural resources from the University of Idaho, Moscow, ID, USA, in 2005 and 2008, respectively.

He is a Research Associate Professor with the Department of Forest Resources, University of Minnesota, Minneapolis, MN, USA. He has been a Faculty with the University of Minnesota, St. Paul, Minnesota, USA, since 2014, and was previously with Michigan Technological University, Houghton, MI, USA. His research interests include remote sensing applications in ecosystem science and management.



Nilam Kayastha received the B.Sc. degree in environmental science from Kathmandu University, Dhulikhel, Nepal, in 2002, the M.Sc. degree in geoinformation science and earth observation from ITC, Enschede, the Netherlands, in 2008, and the Ph.D. degree in geospatial and environmental analysis from Virginia Polytechnic Institute and State University, Blacksburg, VA, USA, in 2013.

She is currently a Research Associate with the Department of Forest Resources, University of Minnesota, Minneapolis, MN, USA. Her research interests include application of geospatial technologies for natural resources assessment and management.



Jean-Philippe Gastellu-Etchegorry received the B.Sc. degree in electrical engineering from ENSEEIHT, Toulouse, France, in 1978, the Aggregation degree in physics from Paris VI University, Paris, France, in 1981, and the two Ph.D. degrees in solar physics in 1983, and remote sensing in 1989 from Paul Sabatier University (UPS), Toulouse, France.

From 1984 to 1990, he worked in PUSPICS, Remote Sensing Center, Gadjah Mada University, Yogyakarta, Indonesia and SEAMEO, Bangkok, Thailand. In 1990, he joined the Centre d'Etude Spatiale des Rayonnements, where he was the Leader of the Remote Sensing Group. In 1995, he joined the Centre d'Etudes Spatiales de la Biosphère (CESBIO, UPS/CNRS/CNES/IRD), Toulouse, France, where he is currently the Deputy Director and Leader of one of the two research teams. He is also Full-Time Professor with UPS. His present research interests include radiative transfer modeling in 3-D turbid, fluid and facet media of the Earth-atmosphere system.



Philip A. Townsend received the Bachelor's degree in history from the University of Virginia, Charlottesville, VA, USA, in 1989, and the Ph.D. degree in geography from the University of North Carolina, Chapel Hill, NC, USA, in 1997.

He is the Vilas Distinguished Achievement Professor of Forest and Wildlife Ecology with the University of Wisconsin-Madison, Madison, WI, USA. He has been a Faculty with the University of Wisconsin, since 2005, and was previously with the University of Maryland Center for Environmental Science, Appalachian Laboratory, Frostburg, MD, USA. His research interests include remote sensing, imaging spectroscopy, and reflectance spectroscopy as related to ecosystem functioning, especially in relation to disturbance, environmental change, and other perturbations